Frontiers in Bioscience Landmark

Front. Biosci. (Landmark Ed) **2025**; 30(10): 45931
https://doi.org/10.31083/FBL45931

Original Research

A Comparative Study of the Effects of Nine CXCR3 Antagonists on Macrophage Function and the Treatment of Acute Lung Injury

Mengjie Zhang[1,†], Ziyu Wan[1,†], Zefeng Zhu[1], Pengbin Wang[1], Xuan Xu[1], Tianhao Ma[1], Feng Qian[2], Lexing Li[3], Guoquan Liu[1], Wei Gu[1,*]

[1]Department of Biochemistry and Molecular Biology, Anhui Provincial Key Laboratory of Tumor Evolution and Intelligent Diagnosis and Treatment, Bengbu Medical University, 233030 Bengbu, Anhui, China
[2]Shanghai Frontiers Science Center of Drug Target Identification and Delivery, Engineering Research Center of Cell & Therapeutic Antibody, Ministry of Education, School of Pharmaceutical Sciences, National Key Laboratory of Innovative Immunotherapy, Shanghai Jiao Tong University, 200240 Shanghai, China
[3]College of Life Science and Technology, Wuhan University of Bioengineering, 430415 Wuhan, Hubei, China
*Correspondence: guwei@bbmu.edu.cn (Wei Gu)
[†]These authors contributed equally.
Academic Editors: Graham Pawelec and Srinivasa Reddy Bonam
Submitted: 20 August 2025 Revised: 4 October 2025 Accepted: 22 October 2025 Published: 31 October 2025

Abstract

Background: The C-X-C motif chemokine receptor 3 (CXCR3) antagonist AMG 487 has been shown to alleviate acute lung injury (ALI) in mice. Other CXCR3 antagonists, including NBI-74330, TAK-779, and SCH 546738, exhibit anti-inflammatory effects in various diseases, including apical periodontitis, arthritis, and acute respiratory distress syndrome (ARDS). However, with the exception of AMG 487, the roles of these antagonists in ALI remain poorly understood. Macrophages can differentiate into various phenotypes and play a crucial role in the progression of inflammatory and autoimmune diseases. **Methods and Results**: In this study, we demonstrate that the CXCR3 agonist C-X-C motif chemokine ligand 10 (CXCL10) enhances macrophage efferocytosis and polarizes inflammatory macrophages toward the M1 phenotype, thereby exacerbating ALI in mice. Conversely, nine CXCR3 antagonists were found to inhibit macrophage efferocytosis and promote the polarization of inflammatory macrophages toward the M2 phenotype, resulting in the alleviation of ALI in mice. Subsequently, molecular docking techniques were employed to analyze interactions between nine CXCR3 antagonists and the CXCR3 protein, with the aim of screening for superior antagonist structures and designing more effective compound configurations targeting the CXCL10-CXCR3 axis. Notably, TAK-779 exhibited the most stable binding affinity to the CXCR3 protein. Furthermore, two newly modified compounds—TAK-779 from imidazolium 1 and TAK-779, 2745583—demonstrated enhanced efficacy compared to the original TAK-779 compound. **Conclusions**: All nine CXCR3 antagonists were shown to influence macrophage function to varying degrees and confer protective effects against ALI. These finding suggest that comparative evaluation of CXCR3 antagonists and the discovery of novel compounds may provide new therapeutic targets for the treatment of inflammatory diseases.

Keywords: acute lung injury; chemokine; CXCR3; CXCL10; CXCR3 antagonist; TAK-779 derivative

1. Introduction

Acute lung injury (ALI) is characterized by increased pulmonary vascular permeability, pulmonary edema, diffuse alveolar damage, and the infiltration of inflammatory cells, including neutrophils and macrophages [1,2]. Chemokines such as CXCL4, CXCL9, CXCL10, and CXCL11, along with their respective receptors, serve as critical mediators of immune cell trafficking and play a pivotal role in both the pathogenesis and resolution of ALI [3]. The overexpression of chemokines can trigger inflammatory diseases, including asthma and atherosclerosis [4,5]. The chemokine receptor C-X-C motif chemokine receptor 3 (CXCR3), a G protein-coupled receptor for the cytokines CXCL9, CXCL10, and CXCL11 [6], participates in tumor progression by regulating tumor growth, migration, invasion, and angiogenesis [7]. Additionally, CXCR3 contributes to the activation of macrophages in mice [8,9]. The CXCL10-CXCR3 axis is pivotal in the immune system, regulating the differentiation, activation, and migration of immune cells [10]. The selective recruitment of cells via CXCL10-CXCR3 can result in tissue damage and exacerbate inflammation. The overexpression of CXCR3 and its ligands is closely linked to pulmonary inflammatory diseases [11,12]. Notably, increased levels of CXCL10 and CXCR3 have been documented in the lung tissues of mice infected with severe acute respiratory syndrome (SARS), influenza virus, and SARS-coronavirus 2 (SARS-CoV-2) [12–14]. Therefore, inhibiting CXCR3 activation may serve as a viable therapeutic target for pulmonary inflammatory diseases.

Macrophages play a crucial role in various inflammatory and autoimmune diseases through both innate and adaptive immunity [15]. An imbalance between the activation and suppression of M1 and M2 macrophage phenotypes has been linked to the pathogenesis of numerous dis-

eases [16]. CXCL10 is essential for macrophage recognition of inflammation. During the early stages of inflammation, $CXCR3^+$ macrophages are recruited to the site of injury by the chemotactic effects of CXCL10, thereby inducing local inflammatory responses. CXCL10 facilitates macrophage migration via the extracellular signal-regulated kinase (ERK) and P38/mitogen-activated protein kinase (P38/MAPK) signaling pathways. The activation of the CXCL10-CXCR3 axis triggers intracellular signaling pathways, including Janus kinase (JAK) and signal transducer and activator of transcription 1 (STAT1), which promote M1 polarization of macrophages and induce inflammatory responses in lung tissue. Inhibition of CXCL10 or CXCR3 secretion can reduce the M1/M2 macrophage ratio and decrease the secretion of inflammatory factors, thereby exerting anti-inflammatory effects [17]. Regardless of whether macrophages are tissue-resident or inflammatory, the same stimulus can elicit distinct responses [18]. The regulation of macrophage polarization by the CXCL10-CXCR3 axis is contingent upon the inflammatory state of the macrophages. In cultured RAW264.7 cells, CXCL10 promotes M2 polarization, whereas the CXCR3 antagonist AMG 487 induces M1 polarization. Conversely, in RAW264.7 cells treated with Poly(I:C), a reagent that simulates viral infection, CXCL10 and AMG 487 induce M1 and M2 polarization, respectively [19]. Previous study has demonstrated that the CXCR3-CXCL10 axis plays a critical regulatory role in both the phagocytic function and polarization of macrophages [20]. CXCL10 enhances the efferocytosis capability of macrophages, while AMG 487 inhibits this function by blocking CXCR3 signaling.

To further elucidate the functions of chemokines and to design therapeutic interventions for ALI, it is crucial to investigate the structural basis of the interactions between chemokines and their receptors [21]. Numerous small-molecule CXCR3 antagonists have been reported, and related medicinal chemistry studies have revealed the molecular properties of these antagonists. For instance, AMG 487 selectively blocks CXCR3 with high efficacy *in vitro* and demonstrates therapeutic effects in a bleomycin-induced murine model of pulmonary inflammation [22]. AMG 487 ameliorated inflammatory changes and pelvic pain in mice with experimental autoimmune prostatitis by reducing Th1 cell differentiation and suppressing M1 macrophage activation [23]. The selective CXCR3 antagonist NBI-74330 reduced neuropathic pain-related behaviors in rats subjected to chronic constriction injury and enhanced the analgesic efficacy of morphine [24]. In low-density lipoprotein receptor-deficient mice treated with NBI-74330, the antagonism of CXCR3 significantly reduced the migration of $CD4^+$ T cells and macrophages to the peritoneal cavity, thereby attenuating the formation of atherosclerotic plaques [25]. The broad-spectrum antagonist TAK-779 effectively blocked the binding of CXCR3 to CXCL10 and inhibited CXCL10-induced cell adhesion and chemotaxis *in vitro* [26]. In a mouse model of SARS-CoV-2-associated acute respiratory distress syndrome (ARDS), TAK-779 suppressed the development of cytokine storms, resulting in a 3–5-fold downregulation of two C-C motif chemokine receptor 5 (CCR5) ligands and macrophage inflammatory proteins (MIP-1α/CCL3 and MIP-1β/CCL4) [27]. SCH 546738 demonstrated a reduction in inflammatory cell infiltration around lesions in a model of apical periodontitis, significantly decreasing the levels of IL-1β, IL-6, and TNF, while also inhibiting the migration of inflammatory cells [28]. The novel small-molecule CXCR3 antagonist, Compound 1 (C1), effectively inhibited CXCR3 (CXCL11)-mediated migration [29]. Hayes *et al.* [30] identified a series of benzimidazole antagonists and evaluated the pharmacokinetic properties of Compound 2 (C2) in mice, demonstrating its favorable bioavailability and half-life following oral administration. A study explored the potential of n-arylpiperazine camphorsulfonamide derivatives as CXCR3 antagonists, where high-throughput screening revealed several competitive and reversible CXCR3 antagonists, including Compound 3 (C3) [31]. Wijtmans *et al.* [32] synthesized and investigated a series of CXCR3 antagonists that feature biphenyl polycyclic fat-anchored quaternary ammonium salts, conducting a functional analysis on Compound 4 (C4). C4 effectively prevented the activation of CXCR3 by CXCL10 [32]. Allen *et al.* [33] identified 1-aryl-3-piperidin-4-ylurea derivatives and analyzed their structure-activity relationships, revealing that Compound 5 (C5) exhibits significant activity with an inhibition constant of 227 nM for mouse CXCR3. The molecular properties of the nine CXCR3 antagonists are summarized in Table 1 (Ref. [7,33–46]).

Multiple CXCR3 antagonists have shown promising therapeutic potential in mitigating inflammatory responses. However, there is currently a lack of relevant research elucidating the mechanisms of action of these CXCR3 antagonists in ALI or conducting a comparative analysis of their effects. This study selected nine CXCR3 antagonists for comparative research, systematically investigating the regulatory effects of CXCL10 and these nine antagonists on macrophage function, while also evaluating their intervention effects on lipopolysaccharide LPS induced ALI in mice. Furthermore, molecular docking technology was employed to analyze the binding interactions between the nine CXCR3 antagonists and the CXCR3 protein, predicting novel structures with more stable binding affinities. This approach may provide new insights and intervention strategies for the clinical treatment of ALI and ARDS.

2. Materials and Methods

2.1 Sources of Nine CXCR3 Antagonists

The CXCR3 antagonists AMG 487, NBI-74330, TAK-779, and SCH 546738 used in this study were purchased from (MedChemExpress, Monmouth Junction, NJ, USA). The compounds C1, C2, C3, C4, and C5 were syn-

Table 1. Molecular properties of nine CXCR3 antagonists.

Compound	Structure	MW	HBA	HBD	RB	AR	Reference
AMG 487	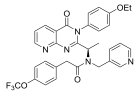	603.6	10	0	10	4	[7,38,39]
NBI-74330	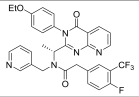	605.6	10	0	9	4	[40,41]
TAK-779	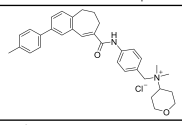	531.1	3	1	6	3	[42–45]
SCH 546738	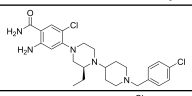	492.4	7	2	6	2	[40,46]
C1	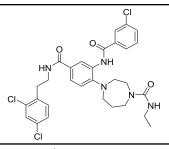	617.0	4	3	8	3	[33]
C2	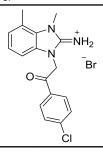	394.7	-	1	-	2	[34]
C3	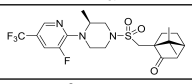	477.5	-	1	-	1	[35]
C4	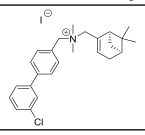	507.9	-	0	-	2	[36]
C5	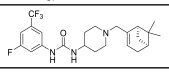	439.5	-	2	-	1	[37]

MW, Molecular weight; HBA, hydrogen bond acceptor; HBD, hydrogen bond donor; RB, rotatable bond; AR, aromatic rin.

thesized based on the literature references provided in Table 1, with specific synthetic routes detailed in **Supplementary Table 1**. Solvents, reagents, and deuterated solvents were purchased from Energy Chemical (Shanghai, China), Aladdin (Shanghai, China), Adamas (Shanghai, China), Innochem (Beijing, China), and were used without further purification. Chemical shifts are expressed in ppm in the δ range, relative to the residual solvent peaks as internal standards: CHCl3 (δ 7.28 by 1H nuclear magnetic resonance [NMR]), CDCl3 (δ 77.0 by 13C NMR). Signal patterns are denoted as: s, single peak; d, double peak; t, triple peak; m, multiple peaks; br, broadened peak. All compounds were subjected to NMR spectroscopy on a Bruker AV400 model, (VANCE NEO 400MHZ, Bruker Biospin AG, Billerica, MA, USA) Silica gel (200–300 mesh) was used for rapid column chromatography (The relevant mass spectra are shown in **Supplementary Table 2**).

2.2 Experimental and Animals

C57BL/6J mice (Qingyuan Biotech, Anhui, China) aged 6–8 weeks and weighing 18–25 g were used in this study. The mice were randomly divided into several groups: a blank control group, a lipopolysaccharide (LPS) group (Sigma, St. Louis, MO, USA), and treatment groups consisting of LPS combined with AMG 487, NBI-74330, TAK-779, SCH 546738, C1, C2, C3, C4, and C5. The number of mice receiving individual drugs or drug combinations was in each case 6 (n = 6 per group). This study was performed following the China Council on Animal Care and Protocol guidelines. All animal studies were conducted in accordance with the guidelines approved by the Ethics Committee for Animal Experiments of Bengbu Medical University (approval number 2021-003) and all applicable institutional and governmental regulations concerning the ethical use of animals were followed.

2.3 Establishment and Treatment of a Mouse Model of ALI

The control and experimental groups received airway injections of phosphate-buffered saline (PBS) (Servicebio, Hubei, China) and lipopolysaccharide (LPS) (10 ng/g) (Sigma, MO, USA), respectively. After 30 h, the mice were anesthetized with tribromoethanol (20 µL/g) (Shang-

hai Dowobio Biotechnology, Shanghai, China). The mice were subsequently euthanized via cervical dislocation, and lung tissues were harvested. The other experimental groups were administered LPS followed by AMG 487 (5 mg/kg), NBI-74330 (5 mg/kg), TAK-779 (10 mg/kg), SCH 546738 (10 mg/kg), C1 (5 mg/kg), C2 (5 mg/kg), C3 (5 mg/kg), C4 (5 mg/kg), and C5 (5 mg/kg). After 24 h, these mice were also euthanized by cervical dislocation, and their lung tissues were collected.

2.4 Pulmonary Ventilation Function Test in Mice

The mouse ALI model and treatment group were established as previously described. Mice were deeply anesthetized with tribromoethanol (20 µL/g) (Shanghai Dowobio Biotechnology, Shanghai, China), after which the trachea was incised, and a tracheal tube was inserted. Lung function changes in the mice were assessed using a lung function ventilator (SCIREQ Scientific Respiratory Equipment Inc., Montreal, Quebec, Canada) and Flexware version 7.6.4 software.

2.5 Collection of Bronchoalveolar Lavage Fluid (BALF) and Total Protein Analysis

Following thoracotomy, the mouse trachea was incised, and the BALF was collected by repeatedly rinsing the lungs with PBS. The samples were centrifuged at 1000 $\times$g for 10 min at 4 °C and both the supernatants and precipitates were collected. The total protein concentration in the BALF samples was determined using a BCA kit (Beyotime, Shanghai, China).

2.6 Cell Culture

Mouse mononuclear macrophages (RAW264.7) were cultured in Gibco Dulbecco's Modified Eagle's Medium (DMEM) (Thermo Fisher Scientific, Waltham, MA, USA), supplemented with 10% fetal bovine serum and 1% penicillin-streptomycin solution (Biosharp, Anhui, China). The cells were incubated at 37 °C in a 5% CO2 atmosphere for 48 h. All cell lines were validated by STR profiling and tested negative for mycoplasma.

2.7 Cell Counting Kit-8 (CCK-8) Detection

RAW264.7 cells were seeded into 96-well plates (1×10^4/well), incubated at 37 °C for 4 h, and treated with nine antagonists at different concentrations (0, 1.0, 2.5, 5.0, 10, 25, 50, and 100 µM) for 24 h. CCK-8 buffer (Beyotime, Shanghai, China) (10 µL) was added to each well in the dark, and the cells were incubated at 37 °C for 0.5, 1, 1.5, and 2 h. The absorbance at 450 nm wavelength was measured using an enzyme counter (Thermo Fisher Scientific, Waltham, MA, USA).

2.8 Neutral Red Phagocytosis Assay

The RAW264.7 cells were stained with 1% neutral red staining solution (Solarbio, Beijing, China). RAW264.7 cells were stained, incubated for 2 h and washed thrice using PBS solution. Cell decolorization solution was prepared by glacial acetic acid and anhydrous ethanol in the ratio of 1:1 to decolorize the stained cells, and the cells were shaken at 4 °C overnight. The absorbance at 540 nm wavelength was detected using an enzyme labeler (Thermo Fisher Scientific, Waltham, MA, USA).

2.9 Protein Immunoblotting Analysis

Mouse lung tissues and cells were lysed using a radioimmunoprecipitation assay (RIPA) lysis solution (Beyotime, Shanghai, China), and the lung tissues were ground with a grinder (Servicebio, Wuhan, China). After sufficient lysis, centrifugation was performed at 4 °C for 10 min at 12,000 rpm, and the supernatant was collected. Protein quantification was conducted using a bicinchoninic acid (BCA) protein concentration assay kit (Beyotime, Shanghai, China). Proteins were separated via 7.5% sodium dodecyl sulfate-polyacrylamide gel electrophoresis and subsequently transferred onto a polyvinylidene difluoride membrane. Blocking was performed with 5% skimmed milk for 2 h. The membranes were then incubated with primary antibodies at 4 °C overnight. After washing three times with tris-buffered saline containing Tween 20 (TBST) buffer (15 min per wash), the membranes were incubated with secondary antibodies at room temperature for 2 h. Following another three washes with TBST buffer (15 min per wash), the membranes were visualized using the Extremely Ultrasensitive ECL Chemiluminescence Kit (Beyotime, Shanghai, China), and protein signals were detected using the Tanon 5200 (Shanghai Tanon Life Science, Shanghai, China). ImageJ software was utilized to analyze the grayscale images. The primary antibodies used were glyceraldehyde-3-phosphate dehydrogenase (GAPDH), β-actin (Beyotime, Shanghai, China), anti-mouse receptor tyrosine kinase (Axl), and anti-mouse protein S (Pros1) (Proteintech, Wuhan, China), while the secondary antibodies included goat anti-rabbit immunoglobulin G (IgG) and goat anti-mouse IgG (Beyotime, Shanghai, China).

2.10 RNA Isolation and Quantitative RT-PCR

Total RNA was extracted from cells using TRIZOL (Biosharp, Anhui, China) and quantified with a Nanodrop spectrophotometer (Thermo Fisher Scientific, Waltham, MA, USA). Subsequently, 1 µL of total RNA was reverse transcribed into single-stranded cDNA at 25 °C for 10 min, followed by 42 °C for 60 min, 80 °C for 10 min, and finally held at 4 °C for 10 min, using a first-strand cDNA synthesis kit (Beyotime, Shanghai, China). PCR was conducted using SYBR-Green PCR Master Mix (Biosharp, Anhui, China), along with specific primers, on a Light Cycler 480 real-time PCR system (Roche Applied Science, Mannheim, Germany). A three-step cycling scheme was employed for gene amplification: 95 °C for 2 min, followed by 95 °C for 10 sec, 58 °C for 30 sec, and 72 °C for 10 sec.

Table 2. Primer sequences.

Gene	Forward sequence (5′-3′)	Reverse sequence (5′-3′)
GAPDH	GGCCTTCCGTGTTCCTAC	TGTCATCATATCTGGCAGGTT
TNF-α	CATCTTCTCAAAATTCGAGTGAC	TGGGAGTAGACAAGGTACAACCC
IL-1β	TGGAAAAGCGGTTTGTCTTC	TACCAGTTGGGGAACTCTGC
IL-6	TAGTCCTTCCTACCCCAATTTCC	TTGGTCCTTAGCCACTCCTTC
CD86	TGTTTCCGTGGAGACGCAAG	TTGAGCCTTTGTAAATGGGCA
CD206	CTTCGGGCCTTTGGAATAAT	TAGAAGAGCCCTTGGGTTGA
Arg1	CTCCAAGCCAAAGTCCTTAGAG	AGGAGCTGTCATTAGGGACATC
Mmp9	GCCGACTTTTGTGGTCTTCC	GGTACAAGTATGCCTCTGCCA
Axl	TGGTGAGGGAGGAGCATGTT	AAAAGAAGGGGAGCTTGCTGA
Pros1	CGCCGTGCAAATACCTTGTT	AATGAGCCAACACGGAATGC
GAS6	TGCTGGCTTCCGAGTCTTC	CGGGGTCGTTCTCGAACAC

The expression levels of specific genes were normalized to that of GAPDH (internal reference), and the fold change was calculated using the $2^{-\Delta\Delta Ct}$ method. The sequences of the gene primers are presented in Table 2.

2.11 Immunofluorescence (IF) Assay

RAW264.7 cells were inoculated onto cell crawlers and incubated for 24 h following 6 h of treatment according to the experimental groups. After three washes with PBS, the cells were fixed in a 4% paraformaldehyde solution for 15 min and subsequently washed three times with PBS. The cells were permeabilized with 0.5% Triton at room temperature for 15 min, followed by three washes in PBS. The cells were incubated for 6 h, and then for an additional 24 h as per the experimental groupings. Blocking was performed using a blocking solution (Beyotime, Shanghai, China) for 30 min, after which the cells were incubated with primary antibodies at 4 °C overnight. The cells were then washed three times with PBS containing Tween 20. Following this, the cells were incubated with a fluorescent secondary antibody (Thermo Fisher Scientific, Waltham, MA, USA) at room temperature in the dark for 2 h, and subsequently washed three times with PBS containing Tween 20. The slices were blocked with a blocking agent containing 4',6-diamidino-2-phenylindole, and fluorescence images were captured using a Zeiss Observer Z1 inverted microscope (ZEISS, Göttingen, Germany) to obtain cell images. The average fluorescence intensity was analyzed using ImageJ software. Primary antibodies (CD86 and CD206) were sourced from AiFang Biological (Hunan, China).

2.12 Histopathologic Examination and Evaluation

Mouse lung tissues were fixed in 5% paraformaldehyde, processed, and embedded in paraffin blocks according to a standard protocol. Tissue sections, each with a thickness of 5 µm, were stained with hematoxylin and eosin. Lung injury was evaluated based on the following criteria: alveolar hemorrhage and congestion, alveolar edema, infiltration or aggregation of neutrophils in the alveolar or vascular regions, and thickening of the alveolar septa. A five-point scale was utilized for scoring: 0 (no lesions or very mild lesions) to 1 (75% lesion extent). The scores were aggregated and reported as the median ± range of injury scores.

2.13 Molecular Docking of Nine CXCR3 Antagonists and CXCR3 Proteins

The corresponding crystal structure of the CXCR3 protein was obtained from the Research Collaboratory for Structural Bioinformatics (RCSB) Protein Data Bank (PDB ID: 8HNM). The protein crystals underwent preprocessing, which included regenerating ligand states, optimizing hydrogen bond assignments, minimizing protein energy, and removing water, all performed using the Protein Preparation Wizard module of Schrödinger software (New York, NY, USA). The two-dimensional (2D) structural data files for AMG 487, NBI-74330, TAK-779, SCH 546738, C1, C2, C3, C4, and C5 were processed using the LigPrep module in Schrödinger software, resulting in the generation of all their three-dimensional (3D) chiral conformations. The Receptor Grid Generation module in Schrödinger software was employed to define the most appropriate enclosing box that perfectly encapsulates the ligand molecules within the 8HNM crystals. Consequently, the active site of the CXCR3 protein was identified. Extra Precision (XP) docking was utilized to molecularly dock the nine processed ligand compounds with the CXCR3 protein's active site. A lower XP score indicates a reduced free energy of binding between the compound and the protein, which correlates with increased binding stability. The XP docking results are evaluated based on the XP GScore, where a value less than –6 signifies stable binding between the ligand and the protein. The active sites of the nine ligand compounds and the CXCR3 protein were further analyzed using molecular mechanics with Generalized Born and Surface Area Solvation (MM-GBSA) calculations, referencing MM-GBSA dG Bind. A value less than –30 kcal/mol suggests that the binding free energy of small molecules to proteins is low, indicating stable binding between the ligands and proteins.

Table 3. Random modification sites and structural modification libraries.

Modification sites	Structural modifier library	
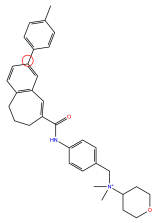	eMolecules R-groups (2098)	R-groups to Create Cation-Pi interaction (96)
	Diverse R-groups (43)	R-groups to Create a Hydrogen Bond (148)
	Solubilizing R-groups (33)	R-groups to Create Pi-Cation Interaction (86)
	Ring Decorations (24)	R-groups to Create Pi-Pi Interaction (86)
	Aliphatic Monocyclic Rings (38)	R-groups to Create Salt Bridges (107)
	Aromatic Monocyclic Rings (73)	R-groups to Replace a Water (139)
	R-groups to Displace a Water (111)	

2.14 TAK-779 Structural Modifications and Subsequent Screening

The 2D structural data file of the TAK-779 compound was processed, and all its 3D chiral conformations were generated using the LigPrep module in Schrödinger software. The R-Group Enumeration module was employed to structurally modify one site of the TAK-779 compound using 13 structural modification libraries (Table 3). The best binding site was predicted using the SiteMap module in Schrödinger software, and subsequently, the Receptor Grid Generation module was utilized to deifne the most suitable Enclosing box to perfectly wrap the predicted binding site. Based on this, the active pocket of the protein was identified. Standard precision (SP) and XP were empolyed to molecularly dock each modified structure with the active site of the CXCR3 protein, with the docking precision being incrementally enhanced. A lower score indicates a higher likelihood of binding between the compound and the protein. The screened modified structures were analyzed in relation to the active site of the CXCR3 protein using MM-GBSA calculations.

2.15 Statistical Analysis

All values are expressed as mean $\pm$ standard deviation. Comparisons between two groups were conducted using a two-sample independent *t*-test, while one-way analysis of variance was employed for comparisons among multiple groups. All statistical analyses were performed using GraphPad Prism 10.0 software (Boston, Massachusetts, USA). *p*-values < 0.05 were considered to indicate statistically significant differences.

3. Results

3.1 CXCL10-CXCR3 Regulates Macrophage Efferocytosis

The IC50 values indicating the effects of nine CXCR3 antagonists on macrophages were determined using the CCK-8 assay (Fig. 1A–I). Treatment of RAW264.7 cells with CXCL10 (300 ng/mL) for 24 h resulted in increased in absorbance and a rise in intracellular neutral red particles within the macrophages. CXCL10 enhanced macrophage phagocytosis (Fig. 2A). The addition of each of the nine CXCR3 antagonists resulted in a reduction in macrophage absorbance, with all treatments significantly suppressing macrophage phagocytosis by over 50%. Among these antagonists, C5 exhibited the most potent inhibition, achieving a 69% reduction (Fig. 2B). CXCL10 upregulated the mRNA expression of efferocytosis-associated molecules Axl, Pros1, and GAS6 (Fig. 2C), while also promoting the protein expression of Axl and Pros1 (Fig. 2D). All nine antagonists significantly downregulated the mRNA expression of Axl and Pros1 (Fig. 2E). Western blot analysis confirmed that these antagonists inhibited the protein expression of both Axl and Pros1 (Fig. 2F,G).

3.2 CXCL10-CXCR3 Regulates Macrophage Polarization

In LPS-induced M1 macrophages responding to CXCL10, mRNA expression levels of M1 polarization markers (TNF-α, IL-1β, and CD86) were all upregulated except for IL-1β. In contrast, all nine CXCR3 antagonists except SCH resulted in varying degrees downregulation of these markers (Fig. 3A). Notably, CXCL10 did not significantly affect the mRNA levels of M2 polarization markers (CD206, Arg1, and Mmp9), while the nine CXCR3 antagonists were found to promote their expression to varying degrees (Fig. 3B). IL-4 induced M2 macrophages, CXCL10 mildly upregulated the M1-polarization-associated molecule CD86. However, all nine antagonists except C1, C3, C4, and C5 downregulated mRNA expression of M1-polarization-associated molecules to varying degrees (Fig. 3C). Conversely, CXCL10 was observed to downregulate the expression of M2 polarization markers, while the antagonists significantly enhanced their mRNA levels to varying degrees (Fig. 3D). In LPS stimulated macrophages, immunofluorescence analysis demonstrated that both LPS and CXCL10 treatments significantly increased CD86 expression compared to the control group. In contrast, all three antagonists (AMG 487, NBI-74330 and C4) reduced CD86 levels, with the C4 group exhibiting the most pronounced suppression (Fig. 3E). Regarding CD206 expression, the LPS group showed no significant change relative to controls, while CXCL10 treatment resulted in a slight decrease. Notably, both AMG 487 and C4 treatments significantly enhanced CD206 expression compared to the LPS group (Fig. 3F). In IL-4 polarized M2 macrophages, CD86 expression was diminished in the IL-4, CXCL10, and all antagonist groups, with the NBI-74330 group demonstrating the strongest inhibition (Fig. 3G). Meanwhile, CD206 levels were elevated

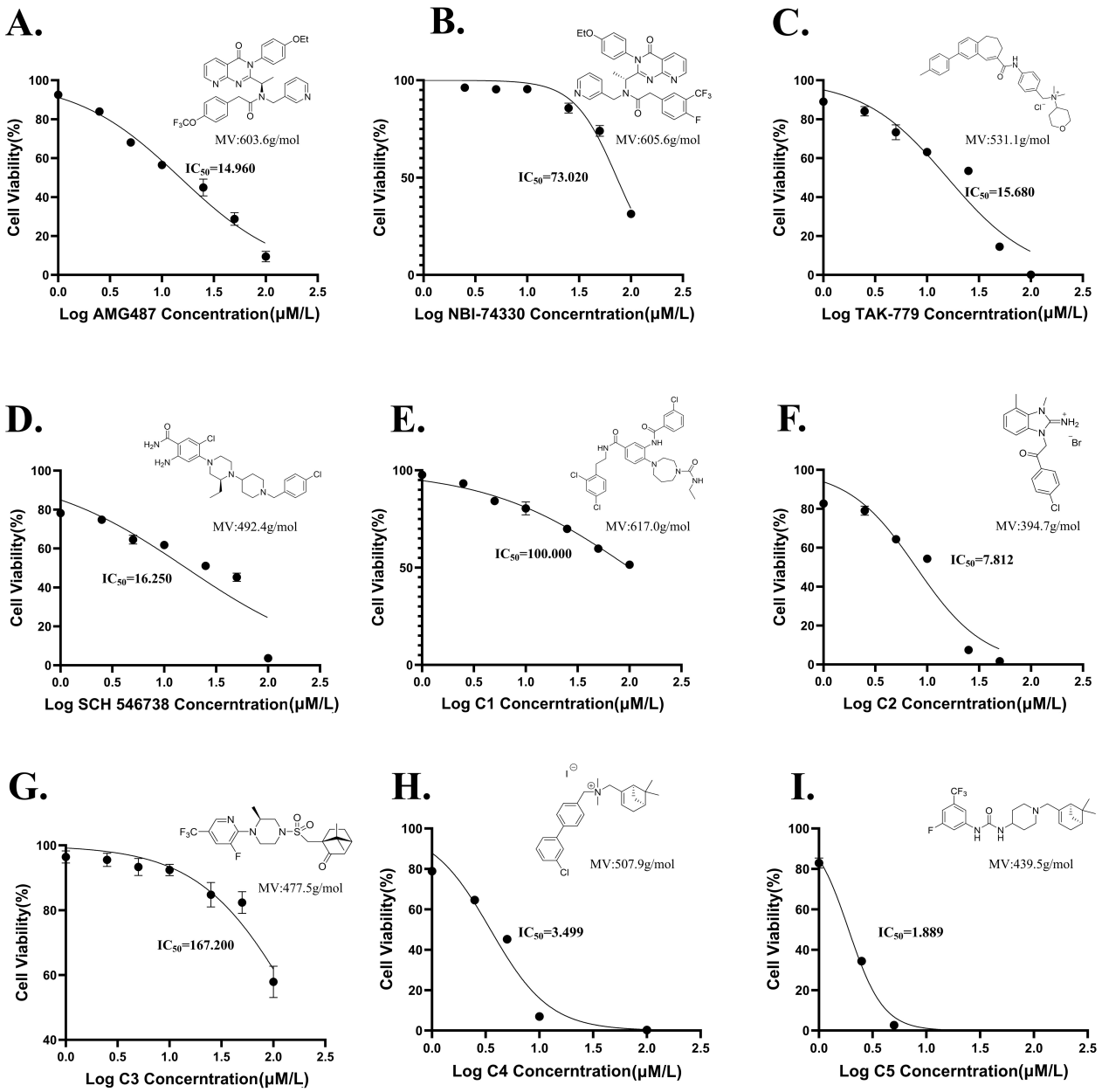

Fig. 1. IC50 values indicating the effects of nine CXCR3 antagonists. (A–I) CCK-8 assay detected the IC50 values indicating the effects of nine CXCR3 antagonists in RAW264.7 cells. Treatment with 14.960 μM AMG 487, 73.020 μM NBI-74330, 15.680 μM TAK-779, 16.250 μM SCH 546738, 100.000 μM C1, 7.812 μM C2, 167.200 μM C3, 3.499 μM C4, and 1.889 μM C5 induced 50% growth inhibition in RAW264.7 cells. CXCR3, C-X-C motif chemokine receptor 3; CCK-8, Cell Counting Kit-8.

in the IL-4 group compared to controls but remained unchanged with CXCL10 treatment. Strikingly, all antagonists further amplified CD206 expression relative to the IL-4 group, with AMG 487 exerting the most robust effect (Fig. 3H).

3.3 CXCR3 Antagonists Alleviate LPS Induced ALI in Mice

In mice with LPS induced ALI, hematoxylin and eosin staining revealed significant structural damage to lung tissue, characterized by thickening of the alveolar walls and diaphragm, as well as pronounced alveolar congestion accompanied by marked infiltration of inflammatory cells and airway hemorrhage. Following the administration of CXCL10, alveolar congestion intensified, and the infiltration of inflammatory cells continued to increase. All nine CXCR3 antagonists effectively mitigated LPS-induced pathological damage in ALI, evidenced by a reduction in inflammatory cell infiltration, improvement in pulmonary hemorrhage and congestion, and preservation of damaged alveolar structures (Fig. 4A). The wet-to-dry (W/D) ratios of mouse lung tissue were utilized to assess the extent of pulmonary edema. The W/D ratio was signif-

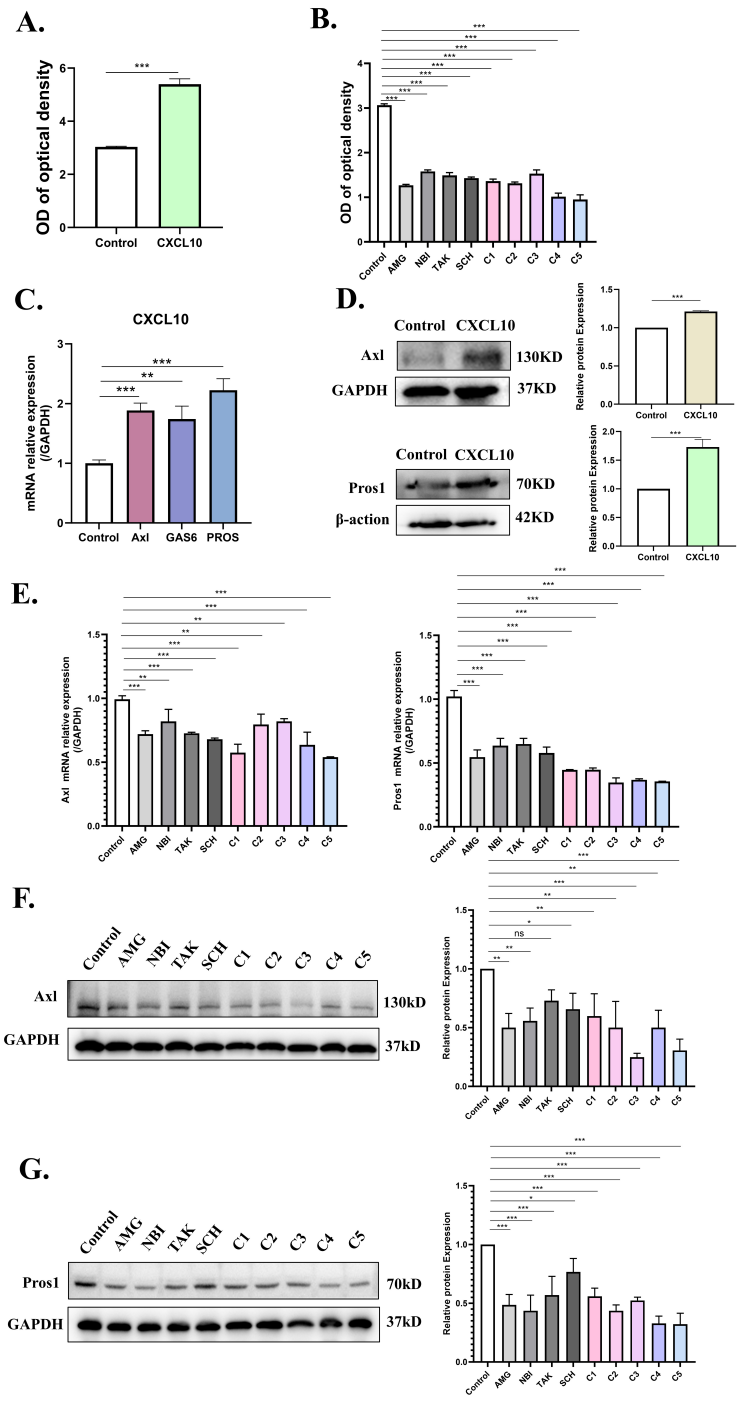

Fig. 2. CXCL10-CXCR3 axis regulates phagocytosis in RAW264.7 cells. (A) Neutral red phagocytosis test detected the phagocytic ability of RAW264.7 cells after CXCL10 stimulation. (B) Neutral red phagocytosis test detected the phagocytic ability of RAW264.7 cells treatment with nine CXCR3 antagonists. (C) The mRNA expression of Axl, GAS6 and Pros1 in RAW264.7 cells after CXCL10 treatment was detected by RT-PCR. (D) Western blotting analysis of Axl and Pros1 proteins in RAW264.7 cells after CXCL10 treatment. (E) The mRNA expression of Axl and Pros1 in RAW264.7 cells after treatment with nine CXCR3 antagonists was detected by RT-PCR. (F) Western blotting analysis of Axl proteins in RAW264.7 cells after treatment with nine CXCR3 antagonists. (G) Western blotting analysis of Pros1 proteins in RAW264.7 cells after treatment with nine CXCR3 antagonists. ns, not significantly different; *$p < 0.05$; **$p < 0.01$; ***$p < 0.001$. N = 3 independent experiments. CXCL10, C-X-C motif chemokine ligand 10.

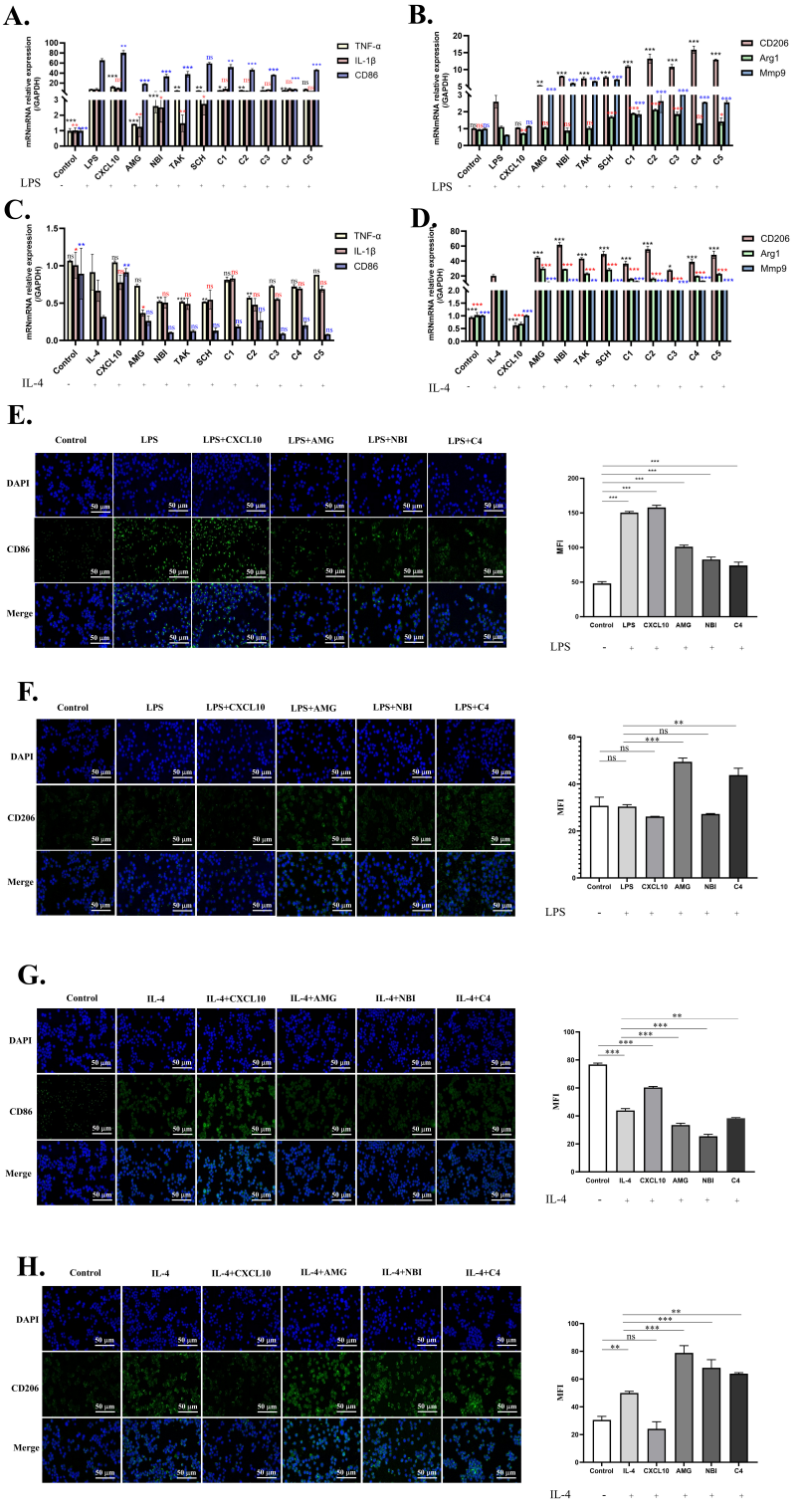

Fig. 3. CXCL10-CXCR3 axis regulates macrophage polarization. (A) LPS (100 ng/mL) treated with RAW264.7 cells, TNF-α, IL-1β and CD86 mRNA expression detected by RT-PCR. (B) LPS (100 ng/mL) treated with RAW264.7 cells, CD206, Arg1 and Mmp9 mRNA expression detected by RT-PCR. (C) IL-4 (20 ng/mL) treated with RAW264.7 cells, TNF-α, IL-1β and CD86 mRNA expression detected by RT-PCR. (D) IL-4 (20 ng/mL) treated with RAW264.7 cells, CD206, Arg1 and Mmp9 expression detected by RT-PCR. (E,F) LPS (100 ng/mL) treated with RAW264.7 cells, the expression of CD86 and CD206 was measured by immunofluorescence. scale bar = 50 μm. (G,H) IL-4 (20 ng/mL) treated with RAW264.7 cells, the expression of CD86 and CD206 was measured by immunofluorescence. scale bar = 50 μm. ns, not significantly different; *$p < 0.05$; **$p < 0.01$; ***$p < 0.001$. N = 3 independent experiments.

Table 4. MM-GBSA analysis of nine CXCR3 antagonists and CXCR3 active sites.

Compound	Target	XP Gscore	MM-GBSA dG Bind (kcal/mol)[2]	MM-GBSA dG Bind Coulomb[1]	MM-GBSA dG Bind Covalent[1]	MM-GBSA dG Bind Hbond[1]	MM-GBSA dG Bind Lipo[1]	MM-GBSA dG Bind Packing[1]	MM-GBSA dG Bind SelfCont[1]	MM-GBSA dG Bind Solv GB[1]	MM-GBSA dG Bind vdW[1]
TAK779		–11.110	–81.31	26.10	2.55	–0.60	–49.72	–6.09	0.00	–2.48	–51.07
C4		–10.351	–74.73	25.77	1.43	0.00	–41.86	–6.56	0.00	–0.36	–53.14
C1		–10.040	–81.48	–15.25	12.39	–1.30	–35.31	–3.88	0.00	37.86	–75.99
NBI74330		–9.713	–52.34	–14.50	7.87	–0.39	–29.64	–6.29	0.00	48.86	–57.73
C5	CXCR3	–8.499	–56.79	–10.36	3.29	–0.10	–31.41	–2.43	0.00	31.49	–47.272
SCH546738		–7.749	–39.89	4.27	11.34	–2.12	–26.65	–3.40	0.00	7.66	–30.99
AMG487		–7.323	–53.11	0.49	3.98	–0.34	–22.90	–3.80	0.00	30.90	–61.42
C2		–6.406	–56.95	73.35	1.41	–0.53	–20.00	–6.88	0.00	–69.55	–34.75
C3		–4.592	–46.40	–8.19	2.83	0.80	–17.34	–0.11	0.00	19.03	–41.82

[1]Coulomb energy, Covalent binding energy, Hydrogen-bonding energy, Lipophilic energy, πPi-pi packing energy, Self-contact correction, Generalized Born electrostatic solvation energy, Van der Waals energy.

[2]MM-GBSA dG Bind = MM-GBSA dG Bind (Coulomb + Covalent + Hbond + Lipo + Packing + SelfCont + Solv GB + vdW).

icantly elevated in the LPS group and was subsequently reduced by all nine CXCR3 antagonists (Fig. 4B). BALF analysis revealed that the administration of LPS resulted in an increase in the total protein content of alveolar lavage fluid in mice, while treatment with the nine CXCR3 antagonists led to a decrease in this total protein content (Fig. 4C). Additionally, RT-PCR results indicated that LPS exposure elevated the mRNA expression levels of inflammatory cytokines TNF-α, IL-6, and IL-1β in mouse lung tissues, with these levels being diminished by the application of the nine CXCR3 antagonists (Fig. 4D). Pulmonary function respirometry revealed significantly elevated tissue elasticity and central airway resistance in the LPS group. Treatment with the nine CXCR3 antagonists markedly reduced the values of these parameters (Fig. 4E and **Supplementary Fig. 1**). Changes in efferocytosis molecules within mouse lung tissues were observed 24 h after treatment with CXCL10 and the nine CXCR3 antagonists. CXCL10 was found to enhance the protein expression levels of Axl and Pros1 (Fig. 4F). Among the nine tested antagonists, five (excluding NBI-74330, C2, C3, and C5) significantly diminished Axl protein expression in murine lung tissue, with C1 exhibiting the most potent inhibitory effect (Fig. 4G). Similarly, eight antagonists (all except AMG 487) downregulated Pros1 protein levels, with TAK-779 demonstrating the strongest suppression (Fig. 4H).

3.4 Interaction of CXCR3 With the Nine Antagonists

The molecular docking scores of the antagonists TAK-779, C4, C1, NBI-74330, and C5 with CXCR3 were found to be –11.110, –10.351, –10.040, –9.713, and –8.499, respectively. Correspondingly, the results of the MM-GBSA analysis yielded values of –81.31, –74.73, –81.48, –52.34, and –56.79 kcal/mol. These low binding free energies and docking scores suggest a very stable binding of all five compounds to the CXCR3 protein. In contrast, the docking scores for the antagonists SCH 546738, AMG 487, and C2 with CXCR3 were –7.749, –7.323, and –6.406, respectively, with their corresponding MM-GBSA results being –39.89, –53.11, and –56.95 kcal/mol. These values also indicate stable binding interactions between these three compounds and the CXCR3 protein. The docking score of antagonist C3 to CXCR3 was found to be –4.596, and the MM-GBSA analysis yielded a result of –46.40 kcal/mol. These values indicate a low free energy of binding and a low docking score, suggesting that the binding of C3 to the CXCR3 protein is relatively unstable. The results of the XP and MM-GBSA analyses are presented in Table 4.

The molecular docking 2D and 3D maps demonstrated that all nine CXCR3 antagonists penetrated deeply into the active pocket of the CXCR3 protein (Fig. 5A–I). The residues of the CXCR3 protein established hydrophobic interactions with the nine antagonists. Notably, residue Tyr308 contributed hydrophobic interactions with AMG 487 (Fig. 5A), NBI-74330 (Fig. 5B), C1 (Fig. 5E), C3 (Fig. 5G), and C5 (Fig. 5I). NBI-74330 formed a hydrogen bond with the residue asparagine (Asn) (Fig. 5B), while TAK-779 established a hydrogen bond with residue serine 304 (Ser304) (Fig. 5C). SCH 546738 formed a hydrogen bond with residue threonine 201 (Thr201) and two hydrogen bonds with residue aspartic acid (Asp) (Fig. 5D). C1 formed hydrogen bonds with residues Arg216 and cysteine 203 (Cys203) (Fig. 5E), C2 established a hydrogen bond with residue Ser304 (Fig. 5F), and C4 formed a hydrogen bond with residue glutamine 204 (Gln204) (Fig. 5G). The interpretation of the docking results is summarized in Table 5.

3.5 Structural Modification and Subsequent Screening of CXCR3 Antagonist TAK-779

Based on the molecular docking results, TAK-779 exhibited the most stable binding affinity to the CXCR3 protein among the nine antagonists evaluated. To identify chemical structures that bind more stably to CXCR3, we modified a specific site in the chemical structure of TAK-779, generating a total of 2128 new structures derived from a library of 13 structural modifications (**Supplementary Table 3**). Of these, 2127 structures demonstrated the ability to interact with the CXCR3 protein. According to the SP docking results, 270 compounds achieved a docking score of $\leq$–8 (**Supplementary Table 4**). These compounds were further subjected to XP screening, using an XP docking score threshold of $\leq$–10 as the screening criterion. The analysis revealed that 65 compounds met this criterion (**Supplementary Table 5**) and were subsequently subjected to MM-GBSA analysis. The XP docking scores of the modified structures of the top 30 ranked compounds along with the results of the free energy of binding obtained from the MM-GBSA are shown in Table 6. The Schrödinger software was utilized to generate 2D maps for the top five ranked chemical modifiers. TAK-779,299968638 established a hydrogen bond with the CXCR3 protein residues Asp99 and Asn132 (Fig. 6A). Similarly, TAK-779,302064729 formed hydrogen bonds with residues Asp99 and Asn132 (Fig. 6B). Additionally, TAK-779 derived from imidazolium 1 interacted with residues Asp297 and Asp278 through hydrogen bonding (Fig. 6C). TAK-779,2745583 established a hydrogen bond with residue Ser304 (Fig. 6D), while TAK-779,529091 formed a hydrogen bond with residue Asp99 (Fig. 6E).

4. Discussion

Chemokines are a class of small molecular proteins primarily responsible for regulating the migration and activation of immune cells. They play significant roles in both innate and adaptive immunity and are involved in processes such as inflammatory responses, immune surveillance, tissue development and repair [34]. The chemokine receptor CXCR3 and certain selective CXCR3 antagonists exhibit varying effects under inflammatory conditions. In lung tis-

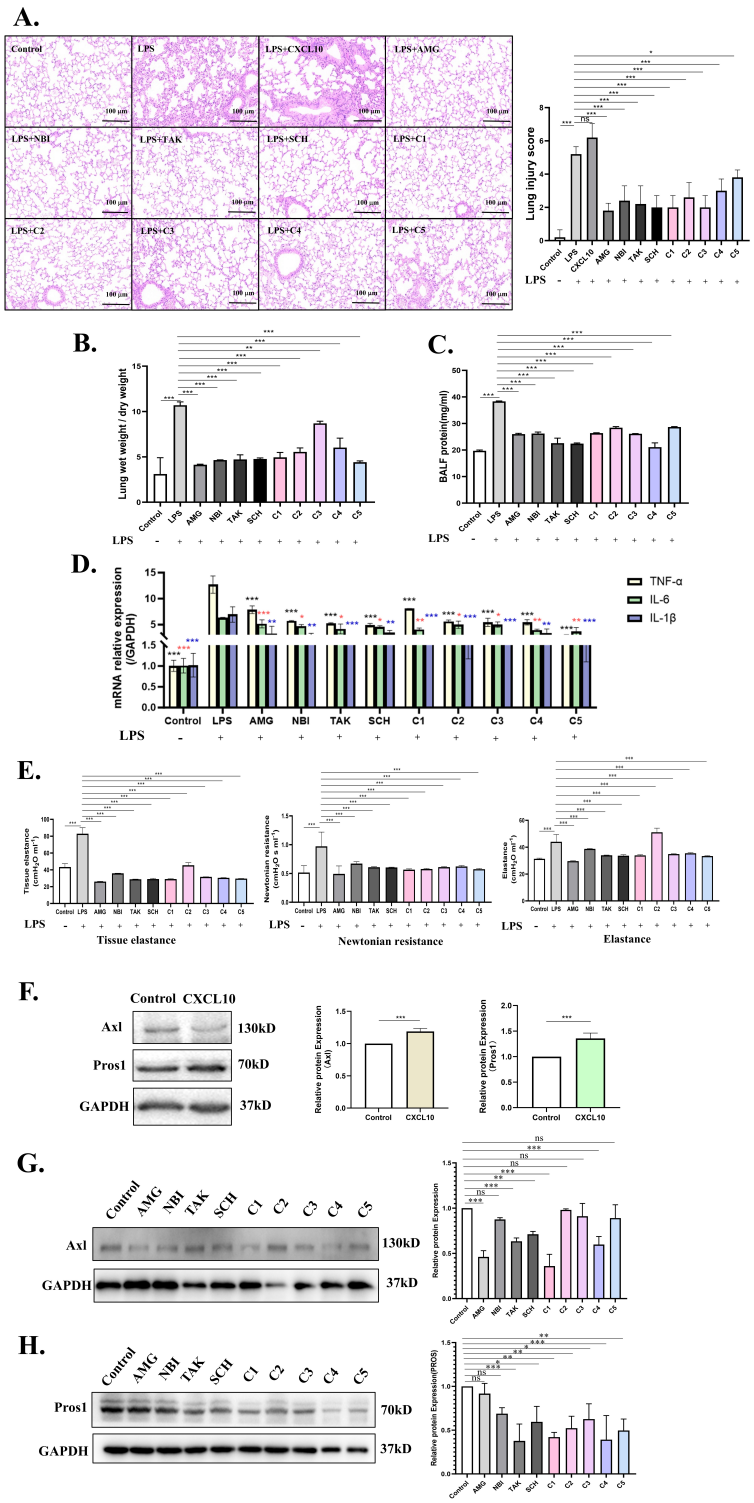

Fig. 4. Nine CXCR3 antagonists alleviate LPS-induced acute lung injury. (A) LPS and treated with CXCL10 and nine CXCR3 antagonists for 24 h. Mouse lung tissues collected for HE stains and lung injury score. scale bar = 100 μm. (B,C) Mouse lung tissues examined for lung wet-to-dry weight ratio and BALF protein. (D) TNF-α, IL-6 and IL-1β inflammatory factors mRNA expression treated with nine CXCR3 antagonists. (E) Lung ventilation assay with nine CXCR3 antagonists, changes in lung respiratory function was detected by tissue elastance, newtonian resistance and resistance. (F) Western blotting analysis of Axl and Pros1 in lung tissues treated with CXCL10. (G,H) Western blotting analysis of Axl and Pros1 in lung tissues treated with nine CXCR3 antagonists. ns, not significantly different; *$p < 0.05$; **$p < 0.01$; ***$p < 0.001$. N = 6 independent experiments.

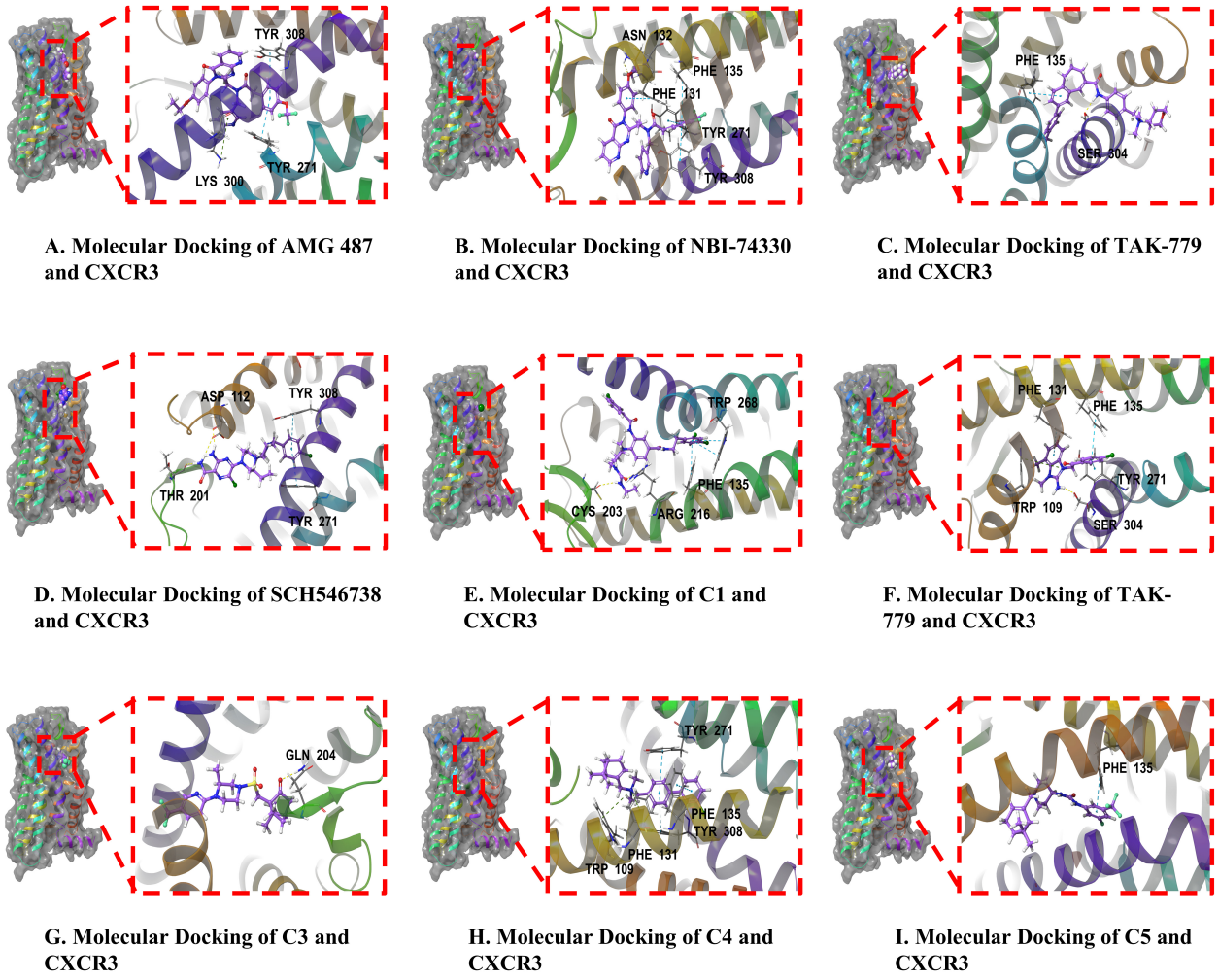

Fig. 5. Binding mode of CXCR3 protein and nine CXCR3 antagonists. (A) AMG 487. (B) NBI-74330. (C) TAK-779. (D) SCH 546738. (E) C1. (F) C2. (G) C3. (H) C4. (I) C5. Yellow, blue, and green represent the hydrogen bond, π-π bond, and π-Cation bond, respectively.

sues of pigs infected with Porcine Reproductive and Respiratory Syndrome Virus (PRRSV), the expression levels of CXCL10 and CXCR3 are elevated. Treatment with the CXCR3 antagonist AMG 487 results in reduced infiltration of inflammatory cells in the alveoli and alleviates lung injury [7]. CXCL10 enhances the mRNA expression of efferocytosis-related molecules, including GAS6, MFGE8, PROS, and Axl, in macrophages. Conversely, the CXCR3 antagonist AMG 487 suppresses the expression of these efferocytosis-related molecules [35]. In RAW264.7 cells treated with Poly(I:C), CXCL10 induces M1-type polarization, whereas AMG 487 promotes M2-type polarization [19]. Despite the discovery of multiple CXCR3 antagonists, there are few clinical trials focusing on these agents. Currently, only the small molecule antagonist AMG 487 has advanced to Phase II clinical trials, although its efficacy remains suboptimal. Various types of CXCR3 antagonists have demonstrated therapeutic effects in animal models of inflammatory diseases. The half-maximal inhibitory concentration (IC50) reflects a drug's inhibitory capability against a specific target or cell type, with lower values indicating stronger inhibitory potency [36]. The varying IC50 values of different antagonists on the same cell primarily highlight the differences in their efficacy. These discrepancies arise from multiple factors, including the distinct mechanisms of action of the antagonists, cellular resistance mechanisms, and the influence of experimental conditions [37,38]. By comparing the IC50 values of various antagonists, more potent drugs can be identified. This comparison of different antagonists' activities allows for the exploration of their structure-activity relationships, which is essential for optimizing drug design and guiding subsequent chemical modifications. Furthermore, different experimental systems may exhibit varying responses to antagonists; thus, screening a diverse range of antagonists enables the selection of the most suitable compound for a specific system, thereby enhancing the reliability and reproducibility of experiments. In this study, we selected nine CXCR3 an-

Table 5. Nine CXCR3 antagonists and CXCR3 protein docking results.

CXCR3 antagonist	CXCR3 protein residue	Binding energy (Kcal/mol)	Hydrogen bonds	Hydrophobic interaction
AMG 487	Tyr60 Leu102 Ala113 Tyr271 Lys300 Tyr308	–9.2	3.85	Leu 56A (3.79 Å)
NBI-74330	Trp109 Asn132 Phe131 Phe135 Tyr-271 Tyr308	–9.6	3.70	Leu 56A (3.73 Å)
TAK-779	Trp109 Ala110 Ala113 Ala114 Phe131 Phe135 Ser304	–9.8	2.90	Leu 49A (3.55 Å)
SCH 546738	Trp109 Asp112 Ala113 Val115 Phe131 Thr207 Tyr271 Tyr308	–8.7	3.22	Trp 109A (3.42 Å)
C1	Leu102 Phe135 Cys203 Arg216 Trp268 Tyr308 Cys311	–9.8	2.57	Tyr 205A (3.55 Å)
C2	Trp109 Phe131 Phe135 Tyr271 Ser304	–8.7	2.40	Trp 109A (3.48 Å)
C3	Tyr60 Trp109 Ala110 Ala113 Gln204 Tyr308	–9.4	2.89	Tyr 205A (3.55 Å)
C4	Leu102 Trp109 Phe131 Phe135 Tyr271 Tyr308 Cys311	–8.2	-	Leu 56A (3.81 Å)

Table 5. Continued.

CXCR3 antagonist	CXCR3 protein residue	Binding energy (Kcal/mol)	Hydrogen bonds	Hydrophobic interaction
C5	Leu106 TRP109 Phe-131 Phe135 Tyr-308	–8.9	1.98	Leu 56A (3.99 Å)

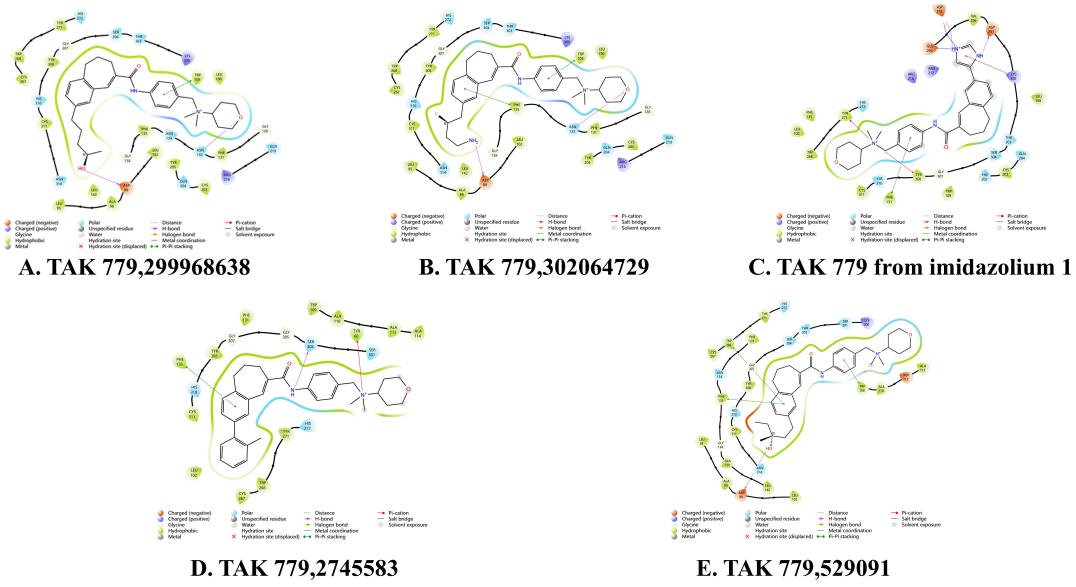

Fig. 6. Binding mode of CXCR3 protein and five TAK-779 modifiers. (A) TAK-779,299968638. (B) TAK-779,302064729. (C) TAK-779 from imidazolium 1. (D) TAK-779,2745583. (E) TAK-779,529091.

tagonist, AMG 487, NBI-74330, TAK-779, SCH 546738, C1, C2, C3, C4, and C5, based on prior findings and relevant literature to comparatively investigate their regulatory effects on macrophage function and their roles in ALI. The selection of various antagonists for the experiments aimed to comprehensively evaluate the biological functions of the CXCR3 target and identify the most effective CXCR3 antagonist. The CCK-8 assay demonstrated that the nine antagonists inhibited the growth of RAW264.7 cells in a dose-dependent manner, exhibiting varying IC50 values.

The process by which both professional and non-professional phagocytes clear apoptotic cells (AC) is referred to as efferocytosis [23]. Macrophages, a pivotal type of phagocyte, are essential for tissue remodeling under normal physiological conditions and for the resolution of inflammation following tissue injury [25]. Furthermore, there is a functional relationship between CXCL10 and the efferocytosis of macrophages. In chronic inflammation, CXCL10 may inhibit the efferocytic function of macrophages by recruiting pro-inflammatory immune cells. This recruitment leads to the accumulation of apoptotic cells and secondary necrosis, thereby exacerbating the inflammatory response. In a mouse model of atherosclerotic plaque formation, both mRNA and protein expression levels of Axl and Pros1 were found to be decreased [39]. Macrophages eliminate apoptotic alveolar interstitial neutrophils through GAS6-dependent expression, suppressing the production of inflammatory cytokines and pulmonary vascular leakage in ALI mice while significantly reducing mortality. This mechanism enables their protective role in inhibiting and resolving inflammation [40]. In this study, we investigated the effects of the CXCR3 agonist CXCL10 and nine CXCR3 antagonists on the efferocytosis function of macrophages. Our findings indicate that CXCL10 enhances macrophage phagocytosis and the expression of molecules associated with macrophage efferocytosis. Conversely, we observed that eight CXCR3 antagonists, NBI-74330, TAK-779, SCH 546738, C1, C2, C3, C4, and C5, suppress macrophage phagocytosis and the expression of efferocytosis-related molecules. This inhibition aligns with the effects of AMG 487 on macrophage phagocytosis and the expression of efferocytosis-related molecules, as documented in previous study [35]. Among the compounds studied, C5 exhibits the most pronounced inhibitory effect, exceeding that of AMG 487. This observation may be attributed to the presence of trifluoromethylphenyl and bicycloheptene structures in C5, which likely enhance its binding affinity to CXCR3. This hypothesis is further supported by molecular docking simulations.

Table 6. MM-GBSA analysis of TAK-779 modifiers.

ID	XP GScore	MM-GBSA dG Bind (kcal/mol)
TAK 779,299968638	–11.390	–66.22
TAK 779,302064729	–11.281	–63.43
TAK 779 from imidazolium 1	–11.250	–87.11
TAK 779,2745583	–11.440	–84.17
TAK 779,529091	–11.138	–54.44
TAK 779 from benzenesulfonamide 2	–11.094	–77.70
TAK 779,40295153	–10.982	–73.65
TAK 779,53752591	–10.944	–47.00
TAK 779,10872246	–10.941	–57.36
TAK 779,537068	–10.931	–77.29
TAK 779,477532	–10.901	–71.75
TAK 779,24179700	–10.898	–71.25
TAK 779 piperidine	–10.852	–53.12
TAK 779,490699	–10.852	–73.46
TAK 779,50418945	–10.837	–78.29
TAK 779,50418945	–10.832	–78.54
TAK 779,724169	–10.790	–73.02
TAK 779,724169	–10.782	–73.27
TAK 779,37212260	–10.761	–43.00
TAK 779,260220769	–10.756	–75.43
TAK 779,44151685	–10.744	–70.03
TAK 779,30485508	–10.740	–60.07
TAK 779,46013797	–10.733	–57.79
TAK 779,6885230	–10.723	–44.25
TAK 779 from piperidinium 1	–10.664	–56.99
TAK 779,7334276	–10.660	–40.54
TAK 779,34736	–10.658	–70.84
TAK 779,2745583	–10.635	–82.27
TAK 779,106287920	–10.629	–78.36
TAK 779 CF2	–10.627	–60.73

LPS can enhance the expression of pro-inflammatory factors and M1 macrophage markers by activating the TLR4 signaling pathway, including the NF-κB and MAPK pathways [41]. In contrast, IL-4 promotes the expression of M2 macrophage markers through the activation of the STAT6 signaling pathway [42]. Our previous study has demonstrated that CXCL10 induces M2 polarization of macrophages, while AMG 487 promotes M1 polarization. However, in macrophages treated with Poly(I:C), an opposite polarization pattern was observed, CXCL10 induced M1 polarization, whereas AMG 487 led to M2 polarization [19]. CD86 and CD206 are surface markers associated with M1 and M2 macrophages, respectively. In LPS-treated alveolar macrophages, the mRNA and protein expressions of TNF-α, IL-6, and iNOS were significantly elevated, indicating a polarization shift of macrophages towards the M1 phenotype. Conversely, following treatment with IL-4, the mRNA and protein levels of IL-10, Arg1, and Mmp9 were significantly increased, resulting in a polarization shift towards the M2 phenotype [43]. This study observed high expression levels of CD86 in macrophages induced by LPS and LPS+CXCL10. Notably, M1 polarization was inhibited in cells pretreated with nine CXCR3 antagonists, with C4 demonstrating the most pronounced inhibitory effect. It was observed that the nine CXCR3 antagonists not only promoted M2 polarization of macrophages but also inhibited M1 polarization, with AMG 487 exhibiting the most pronounced promoting effect. Following IL-4 treatment, there was a notable increase in CD206 expression; however, CXCL10 did not significantly influence CD206 expression. Furthermore, M2 polarization of macrophages was enhanced after pretreatment with the nine CXCR3 antagonists, with AMG 487 again demonstrating the most substantial promoting effect. These findings suggest that the CXCL10-CXCR3 axis plays a regulatory role in determining macrophage polarization. In this study, we focused exclusively on AMG 487, NBI-74330, and C5, and did not conduct immunofluorescence assays on the other six CXCR3 antagonists. As a result, we are unable to accurately ascertain which antagonist exerts the most significant regulatory effect on macrophage M2 polarization. The varying effects of the nine CXCR3 antagonists on macrophage M1/M2 polarization may stem from their distinct regulatory mechanisms, which could be further in-

vestigated through experiments such as signaling pathway analysis and gene knockout studies. Subsequent research could consider employing alveolar macrophages or primary macrophages to further validate the experimental findings presented above.

ALI and ARDS represent clinical syndromes characterized by high morbidity and mortality rates [27]. These conditions can arise from a variety of etiological factors, including shock, severe sepsis, ischemia-reperfusion injury, pulmonary contusion, and severe pneumonia [44]. Currently, there is no specific treatment for ALI or ARDS, highlighting an urgent clinical need for safe and effective therapeutic strategies. A study demonstrated that the combination therapy of pseudoephedrine and emodin significantly inhibited the secretion of inflammatory factors, including TNF-α, IL-6, IL-1β and iNOS, induced by LPS in rats with ALI. Additionally, this therapy promoted the secretion of anti-inflammatory factors such as IL-10 and Arg-1 in BALF and serum [43]. In this study, we utilized an LPS-induced mouse model of ALI to investigate the effects of nine CXCR3 antagonists, AMG 487, NBI-74330, TAK-779, SCH 546738, C1, C2, C3, C4, and C5, on the symptoms of ALI in mice. Our findings showed that these antagonists alleviated ALI symptoms to varying degrees. Notably, the lung injury scoring results indicated that AMG 487 exhibited the most significant therapeutic effect on the lung tissues of mice with ALI. Additionally, the lung W/D ratio demonstrated that AMG 487 was the most effective in reducing pulmonary edema. Furthermore, the assessment of total protein content in BALF revealed that AMG 487 achieved the most substantial recovery of alveolar-capillary barrier function. In mouse lung tissue, all nine CXCR3 antagonists inhibited the mRNA expression of the inflammatory factors TNF-α, IL-6, and IL-1β, with AMG 487 exhibiting the most potent inhibitory effect. The results obtained from both lung tissue and macrophages mutually corroborated each other. However, it is important to note that lung tissue also contains various other cell types, such as epithelial cells, endothelial cells, and fibroblasts, which may influence the experimental results. Previous studies have demonstrated that CXCL10 promotes inflammatory responses, regulates epithelial barrier function, and induces apoptosis in epithelial cells by binding to the CXCR3 receptor and activating associated signaling pathways [45,46]. To accurately interpret the experimental results, further analysis of the role of these cells in lung tissue can be conducted using techniques such as cell separation, gene knockout, or knockdown. In this study, the flexiVent system, widely regarded as the gold standard for invasive respiratory mechanics testing, was utilized to assess various changes in pulmonary function in mice. The experimental results indicated that LPS exposure resulted in a reduction in deep inspiratory capacity, an increase in respiratory resistance, and significant impairment of lung function. All nine CXCR3 antagonists were able to ameliorate these changes to varying degrees. Among them, AMG 487 exhibited the most favorable performance across multiple indicators, including inspiratory capacity, total respiratory system resistance, central airway resistance, and tissue elasticity, demonstrating the most comprehensive improvement in lung function and lung tissue damage. C1, C3, and C4 excelled in specific indicators: static lung compliance, tissue damping, and hysteresis loop area, respectively; however, they were inferior to AMG 487 in all other measured parameters. Therefore, based on the overall efficacy observed in this experiment, AMG 487 emerged as the most effective therapeutic agent for ALI in mice. However, this experiment did not investigate the anti-inflammatory, antioxidant, or other mechanisms of the antagonists in mice, nor did it assess the protective effects of these antagonists at various doses. Additionally, the long-term effects of these antagonists on lung function in animal models were not evaluated. Besides the nine CXCR3 antagonists studied, the newly developed CXCR3 antagonist JN-2 has been shown to inhibit the migration of CXCR3+ bone marrow-derived macrophages and $CD4^+$ T cells, as well as the expression of pro-inflammatory cytokines *in vitro* [47]. ACT-672125 suppresses the recruitment of CXCR3-expressing T cells to inflamed lungs in a dose-dependent manner [48]. Similarly, ACT-777991 exhibits dose-dependent efficacy in a mouse model of acute lung inflammation [49]. The therapeutic blockade of CXCR3 using small molecule antagonists can elucidate the specific role of CXCR3 in chronic inflammatory diseases in detail [50] and provide potential therapeutic strategies for managing these diseases.

In drug development and biomolecular research, understanding the interactions between ligands and receptors is crucial. Key factors influencing ligand-receptor binding include molecular-level aspects such as structure, affinity, and post-translational modifications; cellular-level factors such as receptor expression, internalization, and dimerization; and environmental-level conditions including pH, ion concentration, temperature, mechanical forces, competitive molecules, and extracellular matrix components [51]. These factors collectively determine the efficiency, specificity, and biological function of ligand-receptor binding. A systematic analysis of key regulatory factors elucidates the molecular interaction mechanisms of cellular signal transduction, providing theoretical support at the mechanistic level for the development of targeted drugs and the optimization of clinical treatment pathways. By employing molecular docking technology to analyze the interaction energy between nine antagonists and the CXCR3 protein, we found that TAK-779 exhibits the most stable binding with the CXCR3 protein. Based on the structural framework of TAK-779, we conducted novel structural modifications and subsequent screening for the first time. Our findings reveal that the modified compounds, TAK 779 and TAK 779,2745583, exhibit enhanced binding stability with CXCR3 in comparison to the original compound, TAK-779.

Additionally, we reference alternative synthetic methods for the production of TAK-779 [52,53]. We propose the following possible synthetic routes for the late stage synthesis of TAK-779 from imidazolium 1 and TAK-779,2745583 (**Supplementary Fig. 2**). In our subsequent work, we will further investigate the effects of these two compounds on macrophage function and their roles in LPS induced ALI in mice. We found that the results from macrophages and mouse lung tissues did not align well with the molecular docking results. This discrepancy may be attributed to several factors, including the inherent limitations of molecular docking, the complexity of animal experiments, potential target selection bias, and the properties of the drugs used [54–56]. Future studies could benefit from employing molecular dynamics simulations to further assess the binding stability of the nine CXCR3 antagonists and to refine molecular docking methodologies, thereby minimizing the discrepancies observed between molecular docking and both cellular and animal experiment results. This study revealed that all nine CXCR3 antagonists are capable of regulating macrophage function and alleviating ALI in mice, with AMG 487 exhibiting the most significant therapeutic efficacy. We hypothesize that the combined application of various CXCR3 antagonists may lead to improved therapeutic outcomes in clinical settings. By employing molecular docking technology to examine the interactions between different antagonists and the CXCR3 protein, two superior molecular configurations, TAK 779 from imidazolium 1 and TAK 779, 2745583, were identified through comparative screening. This finding offers new therapeutic insights and strategies for related clinical diseases.

5. Conclusion

CXCL10 enhances macrophage phagocytosis and promotes M1 polarization, whereas CXCR3 antagonists inhibit macrophage phagocytosis and concurrently encourage M2 polarization. Subsequent *in vivo* experiments indicated that all nine tested CXCR3 antagonists conferred protective effects against LPS-induced ALI in mice. Molecular docking analysis revealed that TAK-779 exhibited the most stable binding affinity to the CXCR3 protein. Two superior molecular configurations—TAK-779 from imidazolium 1 and TAK-779, 2745583—demonstrated increased binding stability to CXCR3 compared to the parent compound, suggesting significant optimization potential.

Availability of Data and Materials

Data will be made available on request. The authors confirm that the data supporting the findings of this study are included within the manuscript and its supplementary materials. We adhere to the journal's data sharing policy by making the data freely available. There are no ethical, confidentiality, or legal restrictions preventing the sharing of data from this study.

Author Contributions

WG and GL developed the concept and designed the studies. MZ, ZW, ZZ and PW analyzed the *in vivo* and *in vitro* studies and performed statistical analysis. XX, TM and LL contributed to the experimental studies and data acquisition. FQ and GL contributed to the data analysis and statistical analysis. WG, MZ and ZW wrote and edited manuscript. All authors contributed to editorial changes in the manuscript. All the authors read and approved the final manuscript. All authors have participated sufficiently in the work and agreed to be accountable for all aspects of the work.

Ethics Approval and Consent to Participate

This study was performed following the China Council on Animal Care and Protocol guidelines. All animal studies were conducted in accordance with the guidelines approved by the Ethics Committee for Animal Experiments of Bengbu Medical University (approval number 2021-003) and all applicable institutional and governmental regulations concerning the ethical use of animals were followed.

Acknowledgment

Not applicable.

Funding

This project was supported financially by the Natural Science Research Project of Anhui Educational Committee (2024AH030040), Young and Middle-aged Teacher Development Program of Anhui Educational Committee (JNFX2023029), and the National Natural Science Foundation of China (82104178). Longhu Talent Project of Bengbu Medical University (LH250103005). Innovation Training Program for College Students in Anhui Province, Grants S202410367155 (P. Wang).

Conflict of Interest

The authors declare no conflict of interest.

Supplementary Material

Supplementary material associated with this article can be found, in the online version, at https://doi.org/10.31083/FBL45931.

References

[1] Ning L, Shishi Z, Bo W, Huiqing L. Targeting immunometabolism against acute lung injury. Clinical Immunology (Orlando, Fla.). 2023; 249: 109289. https://doi.org/10.1016/j.clim.2023.109289.

[2] Du M, Wang W, Zhang S, Gu J, Zhang C, Zhang H. SENP1 Promotes Caspase-11 Inflammasome Activation and Aggravates Inflammatory Response in Murine Acute Lung Injury Induced by Lipopolysaccharide. Frontiers in bioscience (Landmark edition). 2024; 29: 397. https://doi.org/10.31083/j.fbl2911397.

[3] Pouzol L, Sassi A, Baumlin N, Tunis M, Strasser DS, Lehembre F, *et al*. CXCR7 Antagonism Reduces Acute Lung Injury Pathogenesis. Frontiers in Pharmacology. 2021; 12: 748740. https://doi.org/10.3389/fphar.2021.748740.

[4] Giuffrida MJ, Valero N, Mosquera J, Duran A, Arocha F, Chacín B, *et al*. Increased Systemic Cytokine/Chemokine Expression in Asthmatic and Non-asthmatic Patients with Bacterial, Viral or Mixed Lung Infection. Scandinavian Journal of Immunology. 2017; 85: 280–290. https://doi.org/10.1111/sji.12532.

[5] van der Vorst EPC, Döring Y, Weber C. Chemokines and their receptors in Atherosclerosis. Journal of Molecular Medicine (Berlin, Germany). 2015; 93: 963–971. https://doi.org/10.1007/s00109-015-1317-8.

[6] Bodnar RJ, Rodgers ME, Chen WCW, Wells A. Pericyte regulation of vascular remodeling through the CXC receptor 3. Arteriosclerosis, Thrombosis, and Vascular Biology. 2013; 33: 2818–2829. https://doi.org/10.1161/ATVBAHA.113.302012.

[7] Liu J, Yao L, Huang S, Wang B, Li L, Li L, *et al*. AMG487 inhibits PRRSV replication and ameliorates lung injury in pig lung xenografts by down-regulating the expression of ANXA2. Antiviral Research. 2022; 202: 105314. https://doi.org/10.1016/j.antiviral.2022.105314.

[8] Qin S, Rottman JB, Myers P, Kassam N, Weinblatt M, Loetscher M, *et al*. The chemokine receptors CXCR3 and CCR5 mark subsets of T cells associated with certain inflammatory reactions. The Journal of Clinical Investigation. 1998; 101: 746–754. https://doi.org/10.1172/JCI1422.

[9] Zhou J, Tang PCY, Qin L, Gayed PM, Li W, Skokos EA, *et al*. CXCR3-dependent accumulation and activation of perivascular macrophages is necessary for homeostatic arterial remodeling to hemodynamic stresses. The Journal of Experimental Medicine. 2010; 207: 1951–1966. https://doi.org/10.1084/jem.20100098.

[10] Tokunaga R, Zhang W, Naseem M, Puccini A, Berger MD, Soni S, *et al*. CXCL9, CXCL10, CXCL11/CXCR3 axis for immune activation - A target for novel cancer therapy. Cancer Treatment Reviews. 2018; 63: 40–47. https://doi.org/10.1016/j.ctrv.2017.11.007.

[11] Saetta M, Mariani M, Panina-Bordignon P, Turato G, Buonsanti C, Baraldo S, *et al*. Increased expression of the chemokine receptor CXCR3 and its ligand CXCL10 in peripheral airways of smokers with chronic obstructive pulmonary disease. American Journal of Respiratory and Critical Care Medicine. 2002; 165: 1404–1409. https://doi.org/10.1164/rccm.2107139.

[12] Ichikawa A, Kuba K, Morita M, Chida S, Tezuka H, Hara H, *et al*. CXCL10-CXCR3 enhances the development of neutrophil-mediated fulminant lung injury of viral and nonviral origin. American Journal of Respiratory and Critical Care Medicine. 2013; 187: 65–77. https://doi.org/10.1164/rccm.201203-0508OC.

[13] Gudowska-Sawczuk M, Mroczko B. What Is Currently Known about the Role of CXCL10 in SARS-CoV-2 Infection? International Journal of Molecular Sciences. 2022; 23: 3673. https://doi.org/10.3390/ijms23073673.

[14] Julian DR, Kazakoff MA, Patel A, Jaynes J, Willis MS, Yates CC. Chemokine-Based Therapeutics for the Treatment of Inflammatory and Fibrotic Convergent Pathways in COVID-19. Current Pathobiology Reports. 2021; 9: 93–105. https://doi.org/10.1007/s40139-021-00226-0.

[15] Navegantes KC, de Souza Gomes R, Pereira PAT, Czaikoski PG, Azevedo CHM, Monteiro MC. Immune modulation of some autoimmune diseases: the critical role of macrophages and neutrophils in the innate and adaptive immunity. Journal of Translational Medicine. 2017; 15: 36. https://doi.org/10.1186/s12967-017-1141-8.

[16] Liu YC, Zou XB, Chai YF, Yao YM. Macrophage polarization in inflammatory diseases. International journal of biological sciences. 2014; 10: 520–529. https://doi.org/10.7150/ijbs.8879.

[17] Zhang J, Liu Y, Chen H, Yuan Q, Wang J, Niu M, *et al*. MyD88 in hepatic stellate cells enhances liver fibrosis via promoting macrophage M1 polarization. Cell Death & Disease. 2022; 13: 411. https://doi.org/10.1038/s41419-022-04802-z.

[18] Sanin DE, Ge Y, Marinkovic E, Kabat AM, Castoldi A, Caputa G, *et al*. A common framework of monocyte-derived macrophage activation. Science Immunology. 2022; 7: eabl7482. https://doi.org/10.1126/sciimmunol.abl7482.

[19] Ye Y, Li L, Kang H, Wan Z, Zhang M, Gang B, *et al*. LAMP1 controls CXCL10-CXCR3 axis mediated inflammatory regulation of macrophage polarization during inflammatory stimulation. International Immunopharmacology. 2024; 132: 111929. https://doi.org/10.1016/j.intimp.2024.111929.

[20] Andrews SP, Cox RJ. Small Molecule CXCR3 Antagonists. Journal of Medicinal Chemistry. 2016; 59: 2894–2917. https://doi.org/10.1021/acs.jmedchem.5b01337.

[21] Power CA, Proudfoot AE. The chemokine system: novel broad-spectrum therapeutic targets. Current Opinion in Pharmacology. 2001; 1: 417–424. https://doi.org/10.1016/s1471-4892(01)00072-8.

[22] Johnson M, Li AR, Liu J, Fu Z, Zhu L, Miao S, *et al*. Discovery and optimization of a series of quinazolinone-derived antagonists of CXCR3. Bioorganic & Medicinal Chemistry Letters. 2007; 17: 3339–3343. https://doi.org/10.1016/j.bmcl.2007.03.106.

[23] Hua X, Zhang J, Ge S, Liu H, Du H, Niu Q, *et al*. CXCR3 antagonist AMG487 ameliorates experimental autoimmune prostatitis by diminishing Th1 cell differentiation and inhibiting macrophage M1 phenotypic activation. The Prostate. 2022; 82: 1223–1236. https://doi.org/10.1002/pros.24395.

[24] Piotrowska A, Rojewska E, Pawlik K, Kreiner G, Ciechanowska A, Makuch W, *et al*. Dataset of (±)-NBI-74330 (CXCR3 antagonist) influence on chemokines under neuropathic pain. Data in Brief. 2018; 21: 1145–1150. https://doi.org/10.1016/j.dib.2018.10.091.

[25] van Wanrooij EJA, de Jager SCA, van Es T, de Vos P, Birch HL, Owen DA, *et al*. CXCR3 antagonist NBI-74330 attenuates atherosclerotic plaque formation in LDL receptor-deficient mice. Arteriosclerosis, Thrombosis, and Vascular Biology. 2008; 28: 251–257. https://doi.org/10.1161/ATVBAHA.107.147827.

[26] Gao P, Zhou XY, Yashiro-Ohtani Y, Yang YF, Sugimoto N, Ono S, *et al*. The unique target specificity of a nonpeptide chemokine receptor antagonist: selective blockade of two Th1 chemokine receptors CCR5 and CXCR3. Journal of Leukocyte Biology. 2003; 73: 273–280. https://doi.org/10.1189/jlb.0602269.

[27] Chernov AS, Rodionov MV, Kazakov VA, Ivanova KA, Meshcheryakov FA, Kudriaeva AA, *et al*. CCR5/CXCR3 antagonist TAK-779 prevents diffuse alveolar damage of the lung in the murine model of the acute respiratory distress syndrome. Frontiers in Pharmacology. 2024; 15: 1351655. https://doi.org/10.3389/fphar.2024.1351655.

[28] Hasegawa T, Venkata Suresh V, Yahata Y, Nakano M, Suzuki S, Suzuki S, *et al*. Inhibition of the CXCL9-CXCR3 axis suppresses the progression of experimental apical periodontitis by blocking macrophage migration and activation. Scientific Reports. 2021; 11: 2613. https://doi.org/10.1038/s41598-021-82167-7.

[29] Cole AG, Stroke IL, Brescia MR, Simhadri S, Zhang JJ, Hussain Z, *et al*. Identification and initial evaluation of 4-N-aryl-[1,4]diazepane ureas as potent CXCR3 antagonists. Bioorganic & Medicinal Chemistry Letters. 2006; 16: 200–203. https://doi.org/10.1016/j.bmcl.2005.09.020.

[30] Hayes ME, Wallace GA, Grongsaard P, Bischoff A, George DM, Miao W, *et al*. Discovery of small molecule benzimida-

zole antagonists of the chemokine receptor CXCR3. Bioorganic & Medicinal Chemistry Letters. 2008; 18: 1573–1576. https://doi.org/10.1016/j.bmcl.2008.01.074.

[31] Wang Y, Busch-Petersen J, Wang F, Kiesow TJ, Graybill TL, Jin J, *et al*. Camphor sulfonamide derivatives as novel, potent and selective CXCR3 antagonists. Bioorganic & Medicinal Chemistry Letters. 2009; 19: 114–118. https://doi.org/10.1016/j.bmcl.2008.11.008.

[32] Wijtmans M, Verzijl D, Bergmans S, Lai M, Bosch L, Smit MJ, *et al*. CXCR3 antagonists: quaternary ammonium salts equipped with biphenyl- and polycycloaliphatic-anchors. Bioorganic & Medicinal Chemistry. 2011; 19: 3384–3393. https://doi.org/10.1016/j.bmc.2011.04.035.

[33] Allen DR, Bolt A, Chapman GA, Knight RL, Meissner JWG, Owen DA, *et al*. Identification and structure-activity relationships of 1-aryl-3-piperidin-4-yl-urea derivatives as CXCR3 receptor antagonists. Bioorganic & Medicinal Chemistry Letters. 2007; 17: 697–701. https://doi.org/10.1016/j.bmcl.2006.10.088.

[34] Baggiolini M. Chemokines in pathology and medicine. Journal of Internal Medicine. 2001; 250: 91–104. https://doi.org/10.1046/j.1365-2796.2001.00867.x.

[35] Hu K, Yingying Y, Guoquan L, Wei G. The role of CXCL10-CXCR3 axis in acute lung injury. Chemistry of Life. 2023; 43: 96–105. https://doi.org/10.13488/j.smhx.20220467.

[36] Tonn GR, Wong SG, Wong SC, Johnson MG, Ma J, Cho R, *et al*. An Inhibitory Metabolite Leads to Dose- and Time-Dependent Pharmacokinetics of (*R*)-*N*-1-[3-(4-Ethoxy-phenyl)-4-oxo-3,4-dihydro-pyrido[2,3-*d*]pyrimidin-2-yl]-ethyl-*N*-pyridin-3-yl-methyl-2-(4-trifluoromethoxy-phenyl)-acetamide (AMG 487) in Human Subjects After Multiple Dosing. Drug Metabolism and Disposition. 2009; 37: 502–513. https://doi.org/10.1124/dmd.108.021931.

[37] Johnson M, Li AR, Liu JW, Fu ZC, Zhu LS, Miao SC, *et al*. Discovery and optimization of a series of quinazolinone-derived antagonists of CXCR3. Bioorganic & Medicinal Chemistry Letters. 2007; 17: 3339–3343. https://doi.org/10.1016/j.bmcl.2007.03.106.

[38] Walser TC, Rifat S, Ma XR, Kundu N, Ward C, Goloubeva O, *et al*. Antagonism of CXCR3 inhibits lung metastasis in a murine model of metastatic breast cancer. Cancer research. 2006; 66: 7701–7707. https://doi.org/10.1158/0008-5472.CAN-06-0709.

[39] Hurtado B, Muñoz X, Recarte-Pelz P, García N, Luque A, Krupinski J, *et al*. Expression of the vitamin K-dependent proteins GAS6 and protein S and the TAM receptor tyrosine kinases in human atherosclerotic carotid plaques. Thrombosis and Haemostasis. 2011; 105: 873–882. https://doi.org/10.1160/TH10-10-0630.

[40] Nepal S, Tiruppathi C, Tsukasaki Y, Farahany J, Mittal M, Rehman J, *et al*. STAT6 induces expression of Gas6 in macrophages to clear apoptotic neutrophils and resolve inflammation. Proceedings of the National Academy of Sciences of the United States of America. 2019; 116: 16513–16518. https://doi.org/10.1073/pnas.1821601116.

[41] Ciesielska A, Matyjek M, Kwiatkowska K. TLR4 and CD14 trafficking and its influence on LPS-induced pro-inflammatory signaling. Cellular and Molecular Life Sciences: CMLS. 2021; 78: 1233–1261. https://doi.org/10.1007/s00018-020-03656-y.

[42] Shi JH, Liu LN, Song DD, Liu WW, Ling C, Wu FX, *et al*. TRAF3/STAT6 axis regulates macrophage polarization and tumor progression. Cell Death and Differentiation. 2023; 30: 2005–2016. https://doi.org/10.1038/s41418-023-01194-1.

[43] Wang WB, Li JT, Hui Y, Shi J, Wang XY, Yan SG. Combination of pseudoephedrine and emodin ameliorates LPS-induced acute lung injury by regulating macrophage M1/M2 polarization through the VIP/cAMP/PKA pathway. Chinese Medicine. 2022; 17: 19. https://doi.org/10.1186/s13020-021-00562-8.

[44] Kaku S, Nguyen CD, Htet NN, Tutera D, Barr J, Paintal HS, *et al*. Acute Respiratory Distress Syndrome: Etiology, Pathogenesis, and Summary on Management. Journal of Intensive Care Medicine. 2020; 35: 723–737. https://doi.org/10.1177/0885066619855021.

[45] Pechkovsky DV, Goldmann T, Ludwig C, Prasse A, Vollmer E, Müller-Quernheim J, *et al*. CCR2 and CXCR3 agonistic chemokines are differently expressed and regulated in human alveolar epithelial cells type II. Respiratory Research. 2005; 6: 75. https://doi.org/10.1186/1465-9921-6-75.

[46] Gao J, Wu L, Wang S, Chen X. Role of Chemokine (C-X-C Motif) Ligand 10 (CXCL10) in Renal Diseases. Mediators of Inflammation. 2020; 2020: 6194864. https://doi.org/10.1155/2020/6194864.

[47] Kim B, Lee JH, Jin WJ, Kim HH, Ha H, Lee ZH. JN-2, a C-X-C motif chemokine receptor 3 antagonist, ameliorates arthritis progression in an animal model. European Journal of Pharmacology. 2018; 823: 1–10. https://doi.org/10.1016/j.ejphar.2018.01.037.

[48] Caroff E, Meyer EA, Äänismaa P, Froidevaux S, Keller M, Piali L. Design, Synthesis, and Pharmacological Evaluation of Benzimidazolo-thiazoles as Potent CXCR3 Antagonists with Therapeutic Potential in Autoimmune Diseases: Discovery of ACT-672125. Journal of Medicinal Chemistry. 2022; 65: 11533–11549. https://doi.org/10.1021/acs.jmedchem.2c00676.

[49] Meyer EA, Äänismaa P, Ertel EA, Hühn E, Strasser DS, Rey M, *et al*. Discovery of Clinical Candidate ACT-777991, a Potent CXCR3 Antagonist for Antigen-Driven and Inflammatory Pathologies. Journal of Medicinal Chemistry. 2023; 66: 4179–4196. https://doi.org/10.1021/acs.jmedchem.3c00074.

[50] Jopling LA, Watt GF, Fisher S, Birch H, Coggon S, Christie MI. Analysis of the pharmacokinetic/pharmacodynamic relationship of a small molecule CXCR3 antagonist, NBI-74330, using a murine CXCR3 internalization assay. British Journal of Pharmacology. 2007; 152: 1260–1271. https://doi.org/10.1038/sj.bjp.0707519.

[51] Wodak SJ, Janin J. Structural basis of macromolecular recognition. Advances in Protein Chemistry. 2002; 61: 9–73. https://doi.org/10.1016/s0065-3233(02)61001-0.

[52] Junker A, Kokornaczyk AK, Zweemer AJM, Frehland B, Schepmann D, Yamaguchi J, *et al*. Synthesis, binding affinity and structure-activity relationships of novel, selective and dual targeting CCR2 and CCR5 receptor antagonists. Organic & Biomolecular Chemistry. 2015; 13: 2407–2422. https://doi.org/10.1039/c4ob02397h.

[53] Junker A, Schepmann D, Yamaguchi J, Itami K, Faust A, Kopka K, *et al*. Diverse modifications of the 4-methylphenyl moiety of TAK-779 by late-stage Suzuki-Miyaura cross-coupling. Organic & Biomolecular Chemistry. 2014; 12: 177–186. https://doi.org/10.1039/c3ob41873a.

[54] Dos Santos Maia M, Soares Rodrigues GC, Silva Cavalcanti AB, Scotti L, Scotti MT. Consensus Analyses in Molecular Docking Studies Applied to Medicinal Chemistry. Mini Reviews in Medicinal Chemistry. 2020; 20: 1322–1340. https://doi.org/10.2174/1389557520666200204121129.

[55] Scarpino A, Ferenczy GG, Keserű GM. Covalent Docking in Drug Discovery: Scope and Limitations. Current Pharmaceutical Design. 2020; 26: 5684–5699. https://doi.org/10.2174/1381612824999201105164942.

[56] Di L, Kerns EH. Application of pharmaceutical profiling assays for optimization of drug-like properties. Current Opinion in Drug Discovery & Development. 2005; 8: 495–504.